Geotechnical Aspects of Underground Construction in Soft Ground – Zhou, Guan & Li (eds)
© 2024 The Author(s), ISBN 978-1-032-53812-9
Open Access: www.taylorfrancis.com, CC BY-NC-ND 4.0 license

3D numerical modelling of a compensation grouting field trial in alluvial soils

D. Boldini & E. Lusini
DICMA, Sapienza University of Rome, Rome, Italy

C. Spaggiari
DISG, Sapienza University of Rome, Rome, Italy

S. Fuoco
INFRARAIL, Florence, Italy

ABSTRACT: The underground bypass of the new high-speed and high-capacity railway line in Florence (IT) involves the construction of about 7 km of twin tunnels beneath the historic city centre. To minimise the impact of tunnelling works, mitigation measures using the compensation grouting technique were integrated into the design stage with the aim of limiting the induced settlements and the risk of damage to nearby structures. A field trial near the *Campo di Marte* railway station was carried out to assess the efficiency of the compensation measure and establish a successful grouting strategy. This paper presents a three-dimensional numerical model of the field trial, explicitly implementing both the grouted volumes and the injection sequence. The grouted area is represented by non-porous soil bulbs with enhanced stiffness properties and the expansion process is simulated through imposed volumetric strains. The injections from each valve of the sleeved pipes (tubes-à-manchettes) are activated in a stepwise procedure, mirroring the injection sequence. The effectiveness of the proposed strategy is validated against recorded displacements in the field trial, demonstrating that the application of non-isotropic volumetric strains (i.e., vertical strains larger than horizontal ones) is able to accurately reproduce the observed heave.

1 INTRODUCTION

The city of Florence (IT), globally renowned for its cultural and historical significance, is undergoing excavation work to improve national mobility and alleviate its impact on the environment. Started in 2023, the construction of a twin-bore tunnel and modern railway station (*Firenze Belfiore*) aims to enhance train transit and reduce journey times along the existing HS/HC railway system, as part of the Scandinavian-Mediterranean Corridor (TEN-T Network).

Given the project location within the city centre, an extensive assessment was conducted on over 230 buildings to identify any potential interference with existing structures and to develop appropriate mitigation strategies, such as compensation grouting, to keep deformations below acceptable thresholds (Zurlo & Sorbello 2022). Furthermore, the interaction between twin tunnel excavation and the *Fortezza da Basso* (a notable Renaissance fortress in the Historic Centre of Florence, listed as a UNESCO World Heritage site from 1982) was investigated using a comprehensive 3D finite element analysis for class-A prediction of the induced level of damage in an optimal tunnel scenario (i.e. considering a surface volume loss of 0.5%) to exclude any potential induced damage (Boldini et al. 2023). As part of the scheduled interventions utilising the compensation grouting technique, preparative works have been initiated involving a compensation field trial close to the *Campo di Marte* railway station, where *Ponte al Pino* is located (Figure 1).

This paper describes the performed Compensation Grouting Trial (CGT) and the 3D numerical model implemented to simulate the grouting process. The proposed method adopts a novel

DOI: 10.1201/9781003413790-19

formulation based on the grout efficiency factor to assess the appropriate strain magnitude to simulate the grout expansion, and aids in gaining further insight into the complex interaction between the volume of injected grout and soil response in terms of vertical displacements.

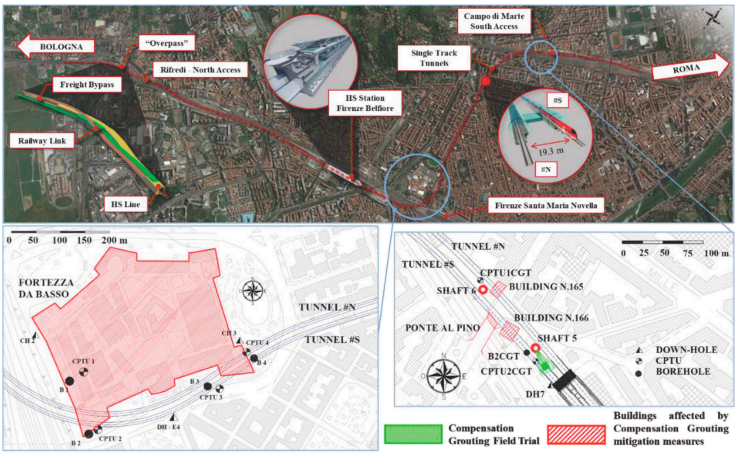

Figure 1. HS/HC Florence bypass project: *Fortezza da Basso* and compensation grouting field trial.

2 THE FIELD TRIAL

2.1 *Site conditions*

The CGT is located in an area characterised by the presence of made ground, gravels in a sandy matrix from the Arno river Supersystem, and silty clays and clayey silts with lenses and layers of gravel from the Florece-Prato-Pistoia lake Supersystem.

Geotechnical characterization was conducted based on the results of site investigations and the laboratory tests closest to the CGT carried out during the 1997 and 2007 campaigns (Figure 1). The site investigation included the borehole B2CGT, two cone penetration tests with piezocone (CPTU1CGT and CPTU2CGT) and a downhole seismic test (DH7). Table 1 synthetizes the 6-layer geotechnical model; the piezometric surface is located at 9 m below the ground surface (42 m a.s.l.) and the pore pressure distribution is hydrostatic. Table 2 summarizes the main

Table 1. Site stratigraphy.

Layer	Elevation (m a.s.l.) from	to	Description
R	51.0	47.5	made ground: coarse-grained material in a silty matrix
LA1	47.5	45.0	silty layer with very consistent clay
SL	45.0	43.0	fine silty-sandy and weakly clayey layer
GSL1	43.0	37.5	gravelly layer in a sandy-silty matrix
LA2	37.5	34.0	silty layer with very consistent clay
GSL2	34.0	28.5	gravelly layer in a silty matrix

Table 2. Properties of the soil layers.

Layer	γ_{dry} (kN/m^3)	γ_{sat} (kN/m^3)	φ' (°)	c' (kPa)	$K_{0,NC}$ (-)	OCR	$K_{0,OC}$ (-)
R	18.5	18.5	41.5	0	0.337	-	0.337
LA1/2	18.5	20.0	25.0	20.0	0.577	2.25	0.813
SL	17.0	17.0	30.5	5.5	0.494	2.85	0.838
GSL1/2	20.0	20.0	45.0	0	0.293	-	0.293

properties of the soil layers. K_0 values for coarse-grained soils were derived from Jaky's equation (1994), while the equation from Mayne & Kulhawy (1982) was used for overconsolidated strata.

2.2 *Methodology and grouting design*

Compensation grouting field trials are commonly employed to calibrate the adequate application of compensation injections (e.g. Sciotti et al. 2012). Additionally, numerical studies have been proposed to simulate the grouting process and to assess its impact. They consist in the application of internal pressure or of volumetric strains to interface or solid elements (e.g. Addenbrooke et al. 2002, Schweiger et al. 2004, Wisser et al. 2005).

Even when considering 3D conditions, a plane state of deformation can be assumed around the TAMs. The volumetric strain, ε_{vol}, to be applied to the cylindrical solid elements, representing the pre-treated soil volumes, can be therefore calculated as in Schweiger et al. (2004), modified after Masini et al. (2014) to account for the different sources of grouting inefficiency:

$$\varepsilon_{vol}=\varepsilon_{zz}+\varepsilon_{xx}=\eta_F\frac{V_{inj}}{\pi a^2}=\frac{\xi}{\eta_S\eta_G}\frac{V_{inj}}{\pi a^2} \tag{1}$$

where V_{inj} is the grout injected volume and a is the radius of the cylindrical solid elements. ξ is the grout efficiency factor that represents the ratio between the surface heave volume generated by the grouting and the volume of the injected material. It is composed of three multiplicative factors: the grout filtration (η_F), the soil compaction (η_S) and the geometry effect (η_G).

According to Nicolini & Nova (2000), the single components of the volumetric strain can be obtained as a function of a size parameter, Δ, here made coincident with ε_{vol} from Equation 1, and a shape parameter, α, varying from 0 (i.e., isotropic expansion) to 1 (i.e., vertical expansion only). This approach allows to account for non-isotropic strains and to identify a preferential direction for the grouting diffusion. Differently from the original formulation, the version here applied considers a plane state of deformation around the cylinder: as such, the strain component along the longitudinal axis of the cylinder, ε_{yy}, is considered as always null and the isotropic part is divided by two instead of three:

$$\begin{cases}\varepsilon_{zz}=\frac{1}{2}(1-\alpha)\varepsilon_{vol}+\alpha\varepsilon_{vol}\\ \varepsilon_{xx}=\frac{1}{2}(1-\alpha)\varepsilon_{vol}\end{cases} \tag{2}$$

where *z* is the vertical direction and *x* is the perpendicular one transversal to the cylinders (Figure 2).

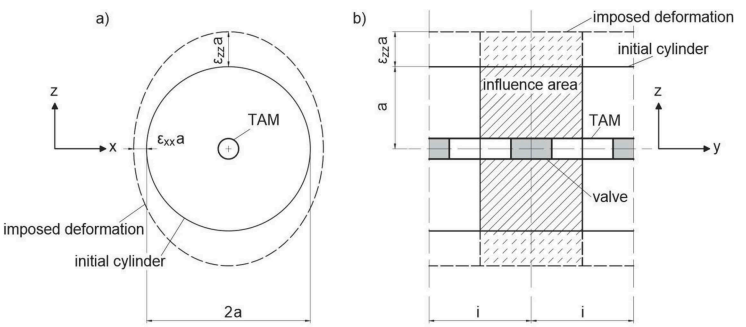

Figure 2. Scheme of the grouting strategy: a) front view (a = radius); b) side view (i= valve inter-axis).

2.3 *Observed behaviour*

The field trial was carried out near shaft no.5 and consisted of two distinct zones formed by two different reinforced concrete (RC) plates. The present study focuses on one of them (RC plate 2),

with a plan size of 8x8 m and an area of influence equal to 240 m^2 (Figure 3). Throughout the testing the vertical displacements of the plate were measured at 9 monitoring points.

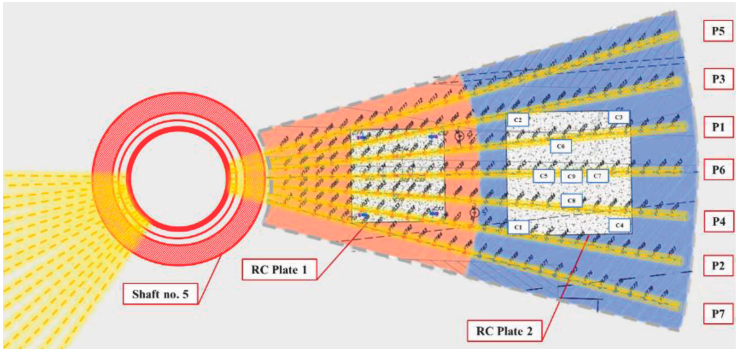

Figure 3. Location of RC plate 2, with TAMs array from shaft no. 5, close to *Campo di Marte*.

The CGT included the following operative phases: installation of tubes-à-manchettes (TAMs), pre-treatment (PT) phase, preliminary (PR) phase, and the proper mitigation phase, subdivided into two further stages (M1 and M2).

The seven TAMs, each with a length of 29.6 m, were installed approximately 7.5 m below the RC plate and arranged in a fan array layout, with each tube containing 26 valves. During the PT phase, a total of 29 m^3 were injected during five different sub-stages. The PR phase was carried out with a uniform simultaneous injection with volumes of 100 l/valve (total injected volume of 4.8 m^3), allowing the estimation of the initial grout efficiency factor (ξ = 9.4 %). This parameter was averaged based on the areas of influence identified around the nine displacement monitoring points on the RC plate.

The subsequent mitigation phase comprised two different stages: a homogeneous one (M1) and a multi-stage phase (M2), involving the application of a differential strategy from different valves depending on the measured heaves. The homogeneous phase resulted in a simultaneous injection of 3.4 m^3 and an estimated ξ of 12.4%, providing the target injected volume for the next phase. In the second stage (corresponding to an injected volume of 1.1 m^3), excessive heave values were recorded, if compared to those expected, especially at the central control points. In addition, a shifting effect of some parts of the plate was observed and the final estimated ξ = 21% value has to be considered as overestimated. It turned out that the process was less controllable as the injections were more differentiated.

Figure 4 shows the response of the RC plate to all the described stages, achieved by conducting Kriging interpolation over the recorded heaves of the control points. In general, an inclined heave can be observed during the pre-treatment and preliminary stages, while progressively higher heaves are recorded at the central points during the mitigation stages. Table 3 lists the measured displacements, total injected volumes per phase, and the calculated grout efficiency factor.

3 FINITE ELEMENT MODELLING

3.1 *The geotechnical model*

The finite element analyses were conducted with the PLAXIS 3D® software (Brinkgrave et al. 2021). A soil domain 120.0×120.0×22.5 m was chosen for minimizing boundary effects. The model reproduces the 6 soil layers and the local hydraulic conditions.

A concrete plate was placed in the centre of the model, resting on the ground surface, with a uniform thickness of 0.1 m. A simple isotropic linear-elastic material model was assigned to the corresponding solid volume (γ = 27 kN/m^3, E = 37 GPa, ν = 0.2). A roughness angle equal to that of the underlying soil was considered for the soil-plate interface.

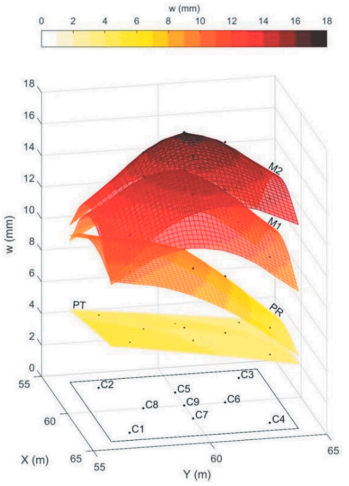

Figure 4. Deformed plate from cumulated control-point (C1–C9) displacements at the end of each injection phase (PT = pre-treatment, PR = preliminary stage, mitigation M1 = 1st stage, M2 = 2nd stage).

Table 3. Incremental vertical displacements per phase and final cumulated displacements at plate control points.

	Vertical displacements (mm)				
Control points	PT	PR	M1	M2	Final
C1	5.7	4.5	1.4	0.9	12.5
C2	4.6	4.9	1.4	1.2	12.1
C3	3.5	1.6	4.8	2.5	12.4
C4	4.3	1.7	4.5	3.7	14.2
C5	4.3	4.7	4.9	2.2	16.1
C6	4.4	3.6	5.5	3.0	16.5
C7	4.9	4.6	4.7	2.4	16.6
C8	5.0	5.5	4.2	1.5	16.2
C9	4.9	5.0	5.0	2.4	17.3
V_{inj} (m^3)	28.9	4.8	3.4	1.1	38.2
ξ (%)	3.0	9.4	12.4	20.9	-

All the soil layers were modelled with the Hardening Soil Model with Small Strain Stiffness (HSsmall), an advanced elastoplastic constitutive model (Benz 2007) which could account for the dependency of soil stiffness on the stress level, its progressive decay with increasing strain level, and the early accumulation of hardening plastic deformations. The profile of small shear strain stiffness, G_0, with depth, z, was determined by calibrating the model parameters G_0^{ref} and $\gamma_{0.7}$ against the down-hole DH7 experimental results (Figure 5). The parameters adopted in HSsmall for different layers are summarised in Table 4. The DH7 experimental profile was slightly adjusted in the vertical direction to align with the soil stratigraphy at the field trial site, which is extremely close to the borehole B2CGT and therefore arguably shares the same stratigraphy.

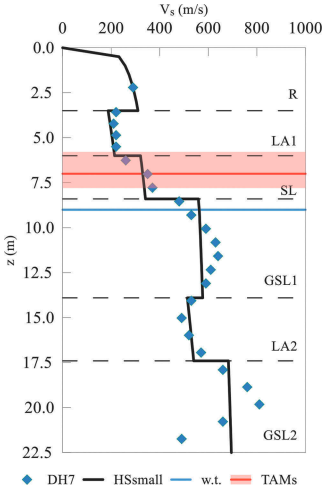

Figure 5. Calibration of HSsmall model from DH7 test results.

Table 4. Soil parameters for HSsmall.

	Soil layer			
Parameters	R	LA1/2	SL	GSL1/2
φ' (°)	41.5	25.0	30.5	45.0
ψ' (°)	0	0	0	0
m (-)	0.3	0.8	0.4	0.2
ν_{ur} (-)	0.2	0.25	0.2	0.2
G_0^{ref} (MPa)	286.8	91.3/318.9	188.72	733.9/998.9
$E'_{ur}{}^{ref}$ (MPa)	137.7	45.6/190.9	90.58	352.3/479.5
$E'_{50}{}^{ref}$ (MPa)	45.9	15.2/63.7	30.19	117.4/159.8
$E_{oed}{}^{ref}$ (MPa)	45.9	15.2/63.7	30.19	117.4/159.8
$\gamma_{0.7}$ (%)	0.01	0.01	0.01	0.01
p^{ref} (kPa)	100	100	100	100
R_f (-)	0.9	0.9	0.9	0.9

3.2 *Modelling of compensation grouting*

The compensation grouting injections were modelled by introducing cylindrical soil volumes with modified stiffness properties around the TAMs, and concurrently applying volumetric strains in the global vertical (ε_{zz}) and x-direction (ε_{xx}). Four of the seven cylinders were completely immersed in the SL layer, the remaining three partly affected the LA1 layer. The soil stiffness inside the cylinders was modified as a function of the intensity of grouting, I_g, defined as the ratio between grout volume (i.e., recorded injected volumes of grout) and the grouted soil volume (i.e., initial cylinder volumes). The TAM arrangement in plan view was derived from technical drawings, with the central TAM oriented along the global y-axis of the model, and the other 6 TAMs arranged as spokes of a wheel, owing to the common origin in the access shaft. They were rotated of 5° to one another, resulting in an overall opening angle of 30° (Figure 6). Each cylinder was 13 m long, subdivided into 13 segments representing the influence volume of each valve (i = 1.0 m).

Following the actual grouting sequence, the analysis was subdivided into 6 consecutive phases. After the initialisation of initial stresses following the K_0 procedure, the concrete plate was activated at the ground surface in the 2nd phase. In the 3rd phase (i.e., the PT phase), the soil cylinders around the TAMs were activated, and their stiffness was modified according to the chart from Falk (1998), considering I_g = 15%. In addition, the unit weight of the cylinders was increased, according to the injected volume, and the volumetric strains were prescribed. In the next three phases, corresponding to the preliminary and mitigation stages, only volumetric strains were applied, as summarised in Table 5, considering the further stiffening and overloading of the grouted soil body as negligible. The last phase (i.e., the M2 phase) was further subdivided into 8 sub-phases, accounting for the real injection sequence of the different groups of valves, as specified in the field-trial technical report (Passante AV, 2012).

Volumetric strains were separately calculated for each valve according to Equations 1-2, starting from the injected volume data for all phases as reported in the technical papers. The subdivision into the z- and x-direction was determined on the basis of simple considerations: i) in the initial stress condition, $K_0 \approx 0.8$ in the LA1 and SL layers, suggested a nearly isotropic subdivision into vertical and horizontal components in PT phase; ii) in the following phases

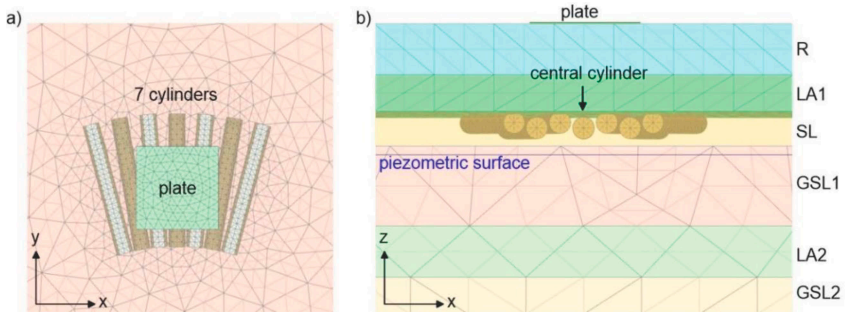

Figure 6. 3D model of the plate and the cylinders: (a) top view, (b) front view.

Table 5. Modifications to the soil parameters inside the cylinders and calibration parameters.

		γ_{unsat} (kN/m^3)		G_0^{ref}($E'_{oed}{}^{ref}$) (MPa)				
Phase		LA1	SL	LA1	SL	ξ (%)	η_F (%)	α (-)
1	Initial	18.5	17.0	91.3(45.6)	188.7(90.58)	-	-	-
2	Plate activation	18.5	17.0	91.3(45.6)	188.7(90.58)	-	-	-
3	PT	21.5	20.0	456.4(228.2)	754.9(362.3)	3.0	5.6	0.0
4	PR	21.5	20.0	456.4(228.2)	754.9(362.3)	9.4	16.5	0.6
5	M1	21.5	20.0	456.4(228.2)	754.9(362.3)	12.4	21.8	0.6
6	M2	21.5	20.0	456.4(228.2)	754.9(362.3)	20.9	36.7	0.6

the proportion was made varying toward a predominant deformation in the vertical direction. This assumption was based on the idea that repeated injections of grout into the soil would eventually result in a stress state in which the effective horizontal stress exceeds the vertical one and preferential horizontal fractures develop (Bezuijen et al. 2011, Falk 1998).

Parameters α and η_F were treated separately: while the first was defined on the basis of theoretical considerations, the second was calibrated in order to obtain a comparable level of displacements with monitoring data at the control points. Laboratory results in silty soils show a η_F in the range 55-85% (Masini et al. 2014), which are expected to further reduce in sandy soil and in field conditions.

3.3 *Results and comparison with field data*

The simulated and measured displacements of the plate were in good agreement at the end of the last mitigation phase (Figure 7a), even if a larger curvature was observed in the FE results, as already noticed in Masini et al. (2014). The absolute difference between maximum displacements, $\delta = w_{simulated} - w_{measured}$, at the end of phase M2 is shown in Figure 7b: the minimum values were about -3 mm (-18%) along two of the four edges of the plate, while for more than 50% of the surface the difference was less than -9% of the measured values (i.e., reconstructed from control points). In Figure 7c the progressive heaving of the plate during all the grouting phases together with the non-uniform deformation of the central cylinder segments is shown. The maximum heave of the plate at C9 is 17.5 mm, about 1% more than the corresponding recorded value.

The simulation of the single phases was not always able to catch the asymmetry of the displacement field induced on the real plate, despite the accurate modelling of (a) the TAMs arrangement, (b) the grout volumes injected per valve and (c) the differential grouting strategy in phase M2. In particular, the simulation did not reproduce the inclination of the plate during the PT and PR phases, when the edge close to C1 and C2 experienced the largest heave. This may be due to the complex stratigraphy in the vicinity of the field trial site, which can be inferred from the analysis of boreholes, and might cause differential displacements and/or affect the permeability around the TAMs and, consequently, the grout efficiency.

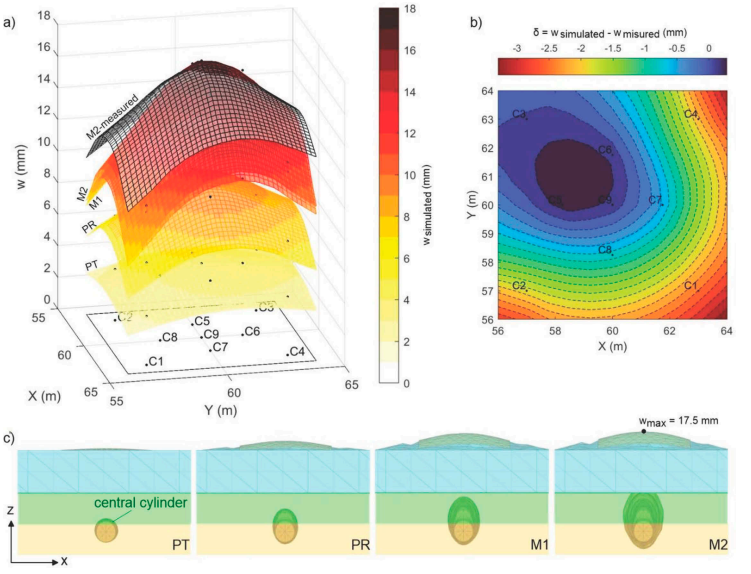

Figure 7. FE results: (a) deformed plate at the end of each injection phase (compared to measured final displacements); (b) difference between simulated and measured displacements (phase M2); (c) deformed mesh of the central cylinder at depth and of the plate at ground surface in all grouting phases.

4 CONCLUSIONS

The paper summarises the numerical modelling of a CG field trial carried out in preparation for the excavation of the high-capacity railway line tunnel below the Florence city centre.

Despite the many practical details of the experimental campaign, the partially simplified numerical procedure was able to capture the displacement field generated by the compensation grouting injections, also thanks to the use of an advanced soil constitutive model properly calibrated in terms of stiffness. While the proposed strategy is highly site-specific and demands careful calibration, it has the potential to assist practitioners in determining the volumes to be injected during full-scale mitigation interventions.

The calibration of injection parameters (i.e. shape factor α and grout filtration efficiency factor η_F) resulting from this study will allow to investigate the effect of compensation grouting in the occurrence of an unlikely critical scenario (i.e. a surface volume loss of 1.5%) during tunnelling below the *Fortezza da Basso*, characterised by similar subsoil conditions. In a unique 3D finite element model, the interaction among tunnelling, soil and structural response, and grouting processes will be simulated, thus permitting a more detailed assessment of the protective effect of the mitigation strategy.

REFERENCES

Addenbrooke, T.I., Ong, J.C.W. & Potts, D.M. 2002. Finite-element analysis of a compensation grouting field trial in soft clay. *Geotechnical Engineering* 155(1): 47–58. 12546.

Benz, T. 2007. Small-strain stiffness of soils and its numerical consequences. PhD thesis. Universität Stuttgart.

Bezuijen, A., te Grotenhuis, R., van Tol, A.F., Bosch, J.W. & Haasnoot, J.K. 2011. Analytical Model for Fracture Grouting in Sand. *American Society of Civil Engineers* 137(6): 611–620

Boldini, D., Spaggiari, C., Abul, J. K., Fuoco, S. & Lusini, E. 2023. Class A predictions of damage level in a historical fortress induced by twin tunnelling. In *Proc. ITA-AITES World Tunnel Congress 2023 (WTC 2023)*, *Athens*, 12-18 May 2023. London: CRC Press. DOI:10.1201/9781003348030-215

Brinkgreve, R.B.J., Kumarswamy, S., Swolfs, W.M., Fonseca, F., Ragi Manoj, N., Zampich, L.M. & Zalamea, N. 2021. *PLAXIS 3D CONNECT* Edition V21.01 Manual. ISBN: 9789076016276

Falk, E. 1998. *Soil improvement by injection of solid material with hydraulic energy*. Ph.D. Thesis, Institut fiir Grundbau und Bodenmechanik, Technische Universitat Wien (in German).

Jaki, J. 1944. The coefficient of earth pressure at rest. *Journal of the Society of Hungarian Architects and Engineers*. 355–358

Nicolini, E. & Nova, R. 2000. Modelling of a tunnel excavation in a non-cohesive soil improved with cement mix injections. *Computers and Geotechnics* 27: 249–272.

Masini, L., Rampello, S. & Soga, K. 2014. An approach to evaluate the efficiency of compensation grouting. J. Geotech. Geoenviron. Eng. 140(12): 04014073. DOI:10.1061/(ASCE)GT.1943-5606.0001180

Mayne, P. V. & Kulhawy, F. H. 1982. K_0–OCR relationships in soil. *Journal of the Geotechnical Engineering Division*. 6: 851–872.

Passante AV, 2012. *Progetto Esecutivo*. Campo prova: relazione di interpretazione finale.

Schweiger, H.F., Kummerer, C., Otterbein, R. & Falk, E. 2004. Numerical modelling of settlements compensation by means of fracture grouting. *Soil and Foundations* 44(1): 71–86.

Sciotti, A., Desideri, A., Saggio, G. & Kummerer, C. 2012. Mitigation of the effects induced by shallow tunneling in urban environment: the use of 'compensation grouting' in the underground Line B1 works in Rome. In *Proc.7th Intern. Symp.*, *Rome*, 16-18 May 2011. London: Taylor & Francis Group.

Wisser, C., Augarde, C.E. & Burd, H.J. 2005. Numerical modelling of compensation grouting above shallow tunnel. *International Journal for Numerical and Analytical Methods in Geomechanics* 29(5): 443–471. DOI:10.1002/nag.421

Zurlo, R. & Sorbello, R. 2022. Florence high-speed railway underpass – Preservation of the Italian Renaissance pre-existing structures and historical sites. In *Proc. 3rd Intern. ISSMGE TC301 Symp.*, *Napoli*, 22-24 June 2022. London: CRC Press.